Atmos. Chem. Phys. Discuss., 13, 24263–24300, 2013
www.atmos-chem-phys-discuss.net/13/24263/2013/
doi:10.5194/acpd-13-24263-2013

Atmospheric Chemistry and Physics Discussions

Primary to secondary organic aerosol: evolution of organic emissions from mobile combustion sources

A. A. Presto, T. D. Gordon, and A. L. Robinson

Center for Atmospheric Particle Studies, Carnegie Mellon University, Pittsburgh, PA, USA

Received: 19 August 2013 – Accepted: 4 September 2013 – Published: 16 September 2013

Correspondence to: A. A. Presto (apresto@andrew.cmu.edu)

Published by Copernicus Publications on behalf of the European Geosciences Union.

Abstract

A series of smog chamber experiments were conducted to investigate the transformation of primary organic aerosol (POA) and formation of secondary organic aerosol (SOA) during the photo-oxidation of dilute gasoline and diesel motor vehicle exhaust. In half of the experiments POA was present in the chamber at the onset of photo-oxidation. In these experiments positive matrix factorization (PMF) was used to determine separate POA and SOA factors from aerosol mass spectrometer data. A two-factor solution, with one POA factor and one SOA factor, was sufficient to describe the organic aerosol in all but one experiment. In the other half of the experiments, POA was not present at the onset of photo-oxidation; these experiments are considered "pure SOA" experiments. The POA mass spectrum was similar to the mass spectra of the hydrocarbon-like organic aerosol factor determined from ambient datasets with one exception, a diesel vehicle equipped with a diesel oxidation catalyst. The SOA in all experiments had a constant composition over the course of photo-oxidation, and did not appear to age with continued oxidation. The SOA mass spectra for the various gasoline and diesel vehicles were similar to each other, but markedly different than ambient oxidized organic aerosol factors. Van Krevelen analysis of the POA and SOA factors for gasoline and diesel experiments reveal slopes of −0.68 and −0.43, respectively. This suggests that the oxidation chemistry in these experiments is a combination of carboxylic acid and alcohol/peroxide formation, consistent with ambient oxidation chemistry. These experiments also provide insight to the mixing behavior of the POA and SOA. Analysis of the time series of the POA factor concentration and a basis-set model both indicate that for all but one of the vehicles tested here, the POA and SOA seem to mix and form a single organic aerosol phase.

ACPD
13, 24263–24300, 2013

1 Introduction

Organic aerosols (OA) comprise roughly 50 % of ambient fine particulate matter (PM) mass (Kanakidou et al., 2005). Understanding the sources and processing of OA is therefore critical to understanding the impacts of PM on climate and human health. Atmospheric OA is commonly classified as either primary organic aerosol (POA), which is directly emitted from combustion and other sources, or secondary organic aerosol (SOA), which results from oxidative atmospheric chemistry (Donahue et al., 2009). SOA dominates the OA burden, ranging from approximately two-thirds of OA mass in urban areas to greater than 90 % of OA mass in downwind and rural areas (Zhang et al., 2007).

Much of what is known about the relative contributions of POA and SOA to ambient OA concentrations is the result of factor analysis of data collected with aerosol mass spectrometers (AMS). Zhang et al. (2005, 2007) used a custom principle component analysis to derive two factors from ambient AMS data (Zhang et al., 2005, 2007). One factor, called hydrocarbon-like OA (HOA), is typically used as a proxy for POA and is defined by a large abundance of m/z 57, specifically $C_4H_9^+$, in the mass spectrum. The mass spectrum of the HOA factor has a high correlation with the OA mass spectrum obtained from fresh diesel engine exhaust (Canagaratna et al., 2004). The second factor, called oxygenated OA (OOA), is associated with ambient SOA and is defined by the large abundance of m/z 44 (CO_2^+) in the mass spectrum. m/z 44 is the primary marker for aerosol oxidation (Canagaratna et al., 2007; Ng et al., 2011a; Zhang et al., 2005, 2007). It is associated with organic acids, and is indicative of highly aged and oxidized aerosol.

More recent work has focused on the use of positive matrix factorization (PMF) to determine OA factor profiles from ambient AMS data sets (Sun et al., 2012; Massoli et al., 2012; Ulbrich et al., 2009; Ng et al., 2010; Huffman et al., 2009; Lanz et al., 2007; Aiken et al., 2009; Docherty et al., 2008; Zhang et al., 2011; Sun et al., 2010). The OA factors derived from PMF analysis can be grouped into three main categories: (1) HOA, (2)

ACPD
13, 24263–24300, 2013

one or more OOA factors, and (3) "specialty" factors associated with biomass burning (Huffman et al., 2009), cooking (Sun et al., 2012), or other sources. The mass spectrum of the HOA factor is generally consistent across many studies and geographic locations, and shares the characteristics, such as a high abundance of the series of $C_nH_{2n+1}^+$ ions, of the HOA factor determined by Zhang et al. (Zhang et al., 2005; Ng et al., 2011b). Most studies define two OOA factors: semi-volatile OOA (SV-OOA), which is thought to correspond with fresh SOA, and low-volatility OOA (LV-OOA), which is thought to correspond with more aged SOA. The mass spectrum of SV-OOA is characterized by m/z 43 ($C_2H_3O^+$) being the most abundant peak; m/z 44 (CO_2^+) is also high in SV-OOA. This is indicative of the early stages of photochemical oxidation (Kroll et al., 2009). The mass spectrum of LV-OOA is dominated by the CO_2^+ ion, suggesting that LV-OOA is at or near the oxidative endpoint for organic aerosol. While SV-OOA and LV-OOA factors share the same basic characteristics across a wide variety of studies, the specific mass spectra seem to be more variable from study to study than the HOA mass spectra (Ng et al., 2010, 2011b; Zhang et al., 2011). This variability is evident in the scatter of ambient SV-OOA and LV-OOA factors when plotted in the "triangle plot" of f_{43} versus f_{44} (Ng et al., 2010).

Two important questions regarding the ambient OA factors determined from PMF analysis are: (1) are the factors physically interpretable, and (2) can the same factors be reproduced in the laboratory? The answer to the first question is "yes". Physical interpretability of the PMF-derived OA factors is a litmus test for determining whether a factor profile is indeed a true factor or is spurious (i.e., the result of operator splitting) (Ulbrich et al., 2009). This manuscript attempts to address the second question.

Numerous smog chamber experiments have investigated the photochemical formation of SOA from dilute combustion exhaust from diesel engines and vehicles (Chirico et al., 2010; Robinson et al., 2007; Sage et al., 2008; Samy and Zielinska, 2010) automobiles, (Nordin et al., 2013; Platt et al., 2012) gas-turbine engines, (Miracolo et al., 2011, 2012) and biomass burning (Grieshop et al., 2009a, b; Hennigan et al., 2011; Heringa et al., 2012). In these experiments, as in the atmosphere, SOA and POA are

ACPD
13, 24263–24300, 2013

present simultaneously. Sage et al. (2008) developed the residual spectrum method to separate the mass spectra of POA and SOA. Much like the custom principle component analysis of Zhang et al. (2005) the residual spectrum analysis assumed that all of the signal at m/z 57 (for a unit mass resolution AMS) was associated with POA, and all of the m/z 44 signal was associated with SOA. Using this method, Sage et al demonstrated that SOA formed from the photo-oxidation of dilute diesel engine exhaust had a similar mass spectrum as ambient oxidized organic aerosol.

One potential flaw of the residual spectrum method is that SOA can also contain signal at m/z 57 as either a reduced ($C_4H_9^+$) or partially oxidized ($C_3H_5O^+$) ion. Chirico et al. (2010) and Miracolo et al. (2010) refined the residual spectrum method using high resolution AMS data and only the reduced ion at m/z 57 ($C_4H_9^+$) as the POA tracer. However, as noted by Chirico, many ions could serve as the POA tracer for the residual method, and the ideal choice of tracer varies for different POA sources. Use of the wrong tracer, such as the use of the entire m/z 57 signal, can significantly over or under estimate the POA concentration in the chamber, and this has a direct impact on the SOA mass spectrum calculated in the residual spectrum.

The work presented in this manuscript seeks to use PMF to improve the estimates of POA and SOA in dilute exhaust smog chamber experiments. PMF has been used sparingly in the analysis of smog chamber data. Craven et al. (2012) used PMF to analyze SOA formed from the photo-oxidation of dodecane, but we are not aware of any applications of PMF to smog chamber experiments using dilute combustion exhaust as the SOA precursor.

In addition to informing the split between POA and SOA (and their respective mass spectra), PMF analysis can also inform OA mixing behavior. Nearly all chemical transport models assume that ambient OA forms a single pseudo-ideal solution and undergoes absorptive partitioning. Gas-particle partitioning is therefore governed by Raoult's

ACPD
13, 24263–24300, 2013

Law (Eq. 1).

$$C_{OA} = \sum_i C_i \left(1 + \frac{C_i^*(T)}{C_{OA}}\right)^{-1} \quad (1)$$

C_{OA} is the total concentration of organic aerosol, and serves as the absorbing medium. Each of the species i can be an individual compound or a lumped surrogate in the Volatility Basis Set (Donahue et al., 2006, 2011, 2012). C^* is the effective saturation concentration ($\mu g\, m^{-3}$), and the temperature dependence of $C^*(T)$ is governed by the Clausius-Clapeyron equation.

Recent research has challenged the notion that all atmospheric OA forms a single mixed organic phase. For instance, Song et al. (2007) observed that the presence of hydrophobic OA seeds did not enhance the SOA mass yield from the ozonolysis of α-pinene. Similarly, several hydrophilic OA seeds, with the exception of citric acid, did not enhance SOA yields either (Song et al., 2011). These results suggested that the SOA was coating, rather than mixing with and partitioning into, the OA seeds. The results of Song et al contrast a series of aerosol mixing experiments by Asa-Awuku et al. (2009), who observed that SOA particles readily mixed with diesel exhaust POA and reached phase equilibrium within several minutes, whereas SOA particles did not mix, or mixed weakly, with lubricating oil particles.

Dilute exhaust smog chamber experiments, where POA is initially present and SOA is formed second, are similar to the experiments presented by Song et al. (2007, 2011). The temporal evolution of PMF-derived SOA and POA factors for these experiments can be used to inform the state of SOA-POA phase mixing in smog chamber experiments.

This paper investigates the composition and evolution of OA as measured by an aerosol mass spectrometer (AMS) for a fleet of gasoline and diesel vehicles. To our knowledge this is the first application of PMF to chamber experiments using dilute combustion exhaust, and therefore the data presented here are a validation of the PMF approach for this type of chamber experiment. Separate POA and SOA factors

ACPD
13, 24263–24300, 2013

are derived for many experiments, and these factors are compared to ambient OA factors derived from PMF. Finally, we use the PMF factors to investigate the mixing between POA and SOA in these experiments.

2 Materials and methods

2.1 Smog chamber experiments

The experiments presented here are similar to previous tests of SOA production from gas-turbine engines (Miracolo et al., 2011, 2012) and biomass burning (Hennigan et al., 2011) presented by this group using the same portable smog chamber and instrumentation suite. In a set of companion papers, Gordon et al. (2013a, b) present full analyses of SOA production from the gasoline and diesel vehicles presented here.

All experiments were conducted at the California Air Resources Board's (CARB) Haagen-Smit Laboratory (HSL). The vehicle fleet considered here consisted of 3 LEV-1 automobiles, 4 LEV-2 automobiles, and two diesel vehicles. The California LEV-1 standards cover vehicles for model years 1994–2003, and LEV-2 covers model years 2004–2012. The model years of the specific vehicles tested for this study range from 1996 to 2010. The vehicles and model years are listed in Table 1. The make and model of each vehicle has been redacted and replaced with a code indicating the control level or fuel (LEV1, LEV2, or D), a numerical indicator for the vehicle, and a test number for the vehicle. For example, test LEV1-1.5 was the fifth test with vehicle LEV1-1. The vehicle fleet considered here is a subset of a larger fleet; full details of the entire vehicle fleet and the full suite of testing procedures are available elsewhere (Gordon et al., 2013a, b; May et al., 2013a, b, c).

Vehicles were tested on a chassis dynamometer using a cold-start Unified Cycle (UC). Figure S.1 (Supplement) shows the speed trace for the UC. The UC has a three-phase structure, with 1435 s (28.9 min) of driving time and a total distance of 17.6 km

ACPD
13, 24263–24300, 2013

(11 mi). The first two phases of the UC are run consecutively, followed by a ten-minute, engine-off hot soak, and then a repeat of phase 1.

Emissions were sampled from the vehicle tailpipe using a constant volume sampler (CVS). A slipstream of the diluted emissions from the CVS was transferred into a portable smog chamber at a constant flow rate (16 lpm) using two Dekati ejector dilutors. The dilution ratio in the ejector dilutors was 8–10 : 1. The transfer line was 12 m long, constructed out of electrically heated (47 °C), 1.27 cm (0.5 in) O.D. Silcosteel tubing. The Dekati ejector diluters were also heated to 47 °C and operated on HEPA- and activated-carbon-filtered air.

The smog chamber was a 7 m^3 Teflon chamber (Hennigan et al., 2011; Miracolo et al., 2011, 2012; Presto et al., 2011). Before each experiment the chamber was cleaned by flushing with HEPA- and activated carbon-filtered air overnight. The chamber was cleaned to less than 10 particles cm^{-3} and < 5 ppb NO_x. The smog chamber was located indoors, in a large air-conditioned space; its temperature and humidity varied between 25–32 °C and 30–50 %.

Dilute vehicle emissions from the CVS were continuously added to the chamber over the entire UC but not during the 10 min hot soak period. After filling, the exhaust inside the chamber was a factor of 200–300 more dilute than the conditions at the tailpipe and PM concentrations were typically within the range of urban ambient conditions (< 10 µg m^{-3}) for all of the gasoline vehicles. In some diesel tests, primary PM concentrations were as high as 80 µg m^{-3}, though much of this mass was black carbon. The mixing ratios of individual VOCs inside the chamber were typically less than 1 ppb, but were as high as 20 ppb for the highest emitting vehicle. The NO_x concentrations inside the chamber after filling were between 0.1 and 2.4 ppm. Additional details are available in Gordon et al. (2013a, b).

After adding exhaust, nitrous acid (HONO) was introduced into the chamber as an OH radical source. VOC : NO_x ratios were adjusted to approximately 3 : 1 by the addition of propene. Several experiments with VOC : NO_x ratios ranging from 0.25 to 1.16 were also performed to investigate the impact of this parameter on SOA formation (e.g.,

ACPD
13, 24263–24300, 2013

experiments LEV1-6.3, D4.2, D5.1). After ∼45 min of characterization of the primary emissions in the dark, the emissions were photo-oxidized by exposing them to UV lights (Model F40BL UVA, General Electric) continuously for 3 h.

A suite of instruments was used to characterize gas- and particulate-phase pollutants inside the chamber. Full details on the suite of instruments coupled to the smog chamber is available in Gordon et al. (2013a, b). This manuscript focuses on analysis of quadrupole AMS data obtained at unit mass resolution (Canagaratna et al., 2007; Jayne et al., 2000). The fragmentation table of Allan et al. (2004) was used to interpret the AMS data. The contribution of gas-phase CO_2 to the AMS m/z 44 signal was corrected using measured CO_2 concentrations as a function of time. There was no evidence of organic particle signal at m/z 28 (CO^+) either before or after the start of photo-oxidation. The particulate nitrate signal was apportioned between organic and inorganic nitrates using the approach of Farmer et al. (2010). A minor fraction (typically <5 %) of the nitrate mass was attributable to organics.

The experiments in Table 1 can be grouped into two categories. In half of the experiments ($N = 8$), there was not an appreciable POA concentration ($<0.5\,\mu g\,m^{-3}$) in the smog chamber after filling with dilute exhaust. These experiments are considered "pure SOA" experiments, and PMF was not required. POA was present in the remaining half of the experiments ($N = 8$). For these experiments, Positive Matrix Factorization (Paatero, 1997; Paatero and Tapper, 1994) was used to deconvolve POA and SOA factors. The PMF analysis of AMS data followed the method and tools outlined by Ulbrich et al. (2009).

2.2 Basis set modeling

A model was constructed to investigate the partitioning behavior of the POA factors determined from PMF analysis. The model uses the one-dimensional volatility basis set with logarithmically-spaced bins of C^* (Donahue et al., 2006). Inputs to the model were: temperature, wall loss corrected organic aerosol concentration (C_{OA}, $\mu g\,m^{-3}$), OH radical concentration, the first-order rate constant for the reaction of low volatility vapors

ACPD
13, 24263–24300, 2013

with OH (k_{OH}), the volatility distribution (f_i) of the POA, and the first-order wall loss rate constant in the chamber. Temperature was measured in the chamber, and C_{OA} was determined by wall-loss correcting the total organic aerosol mass reported by the AMS. Wall loss corrections were performed using the ratio of OA to black carbon, where the latter serves as a conserved wall-loss tracer (Hildebrandt et al., 2009; Grieshop et al., 2009b). OH radical concentrations were estimated from the decay of VOCs using the PTR-MS (Gordon et al., 2013a, b; Miracolo et al., 2012, 2011) and k_{OH} was assumed to be 3×10^{-11} molecule^{-1} cm^3 s^{-1} (Atkinson and Arey, 2003). The volatility distribution of the POA for the volatility range $10^{-2} \le C^* \le 10^6$ was determined from GC-MS analysis of quartz filter samples collected from the CVS (May et al., 2013a, b), following the method of Presto et al. (2012).

Two modeling cases are considered. Case 1 assumes ideal mixing between the POA and SOA. Case 2 assumes that the POA and SOA form distinct organic phases that do not mix. The models are identical in the pre-oxidation (t<0) period, when all of the OA is present as POA (i.e., C_{OA} is the POA concentration). C_{OA} and f_i are used to calculate the POA and vapor concentration in each volatility bin according to Eq. (1).

After the start of photo-oxidation (t>0), the vapors in each C^* bin (C_i^{VAP}) react with OH with first-order kinetics:

$$\frac{dC_i^{VAP}}{dt} = -k_{OH}[OH][C_i^{VAP}] \quad (2)$$

The model only considers primary vapors (vapors associated with POA), and does not aim to predict the extent of SOA formation. The vapors that react with OH therefore leave the system, and are removed from the overall mass balance. Heterogeneous reactions of condensed-phase organics with OH are not considered in the model.

The reaction of organic vapors with OH perturbs gas-particle equilibrium, which is subsequently recalculated using Eq. (1). In modeling Case 1, the POA and SOA are assumed to form an ideal mixture. Thus the total absorbing phase is the calculated C_{OA}, and the gas-particle partitioning of the POA is calculated accordingly. In Case 2,

ACPD
13, 24263–24300, 2013

the POA and SOA are assumed to form distinct phases that do not mix; thus the total concentration of the POA-absorbing phase is the POA alone. It is further assumed that there is no mass transfer resistance to POA evaporation through a coating of SOA. Since the gas-phase chemistry continually strips away the vapors from above the POA, the POA in Case 2 always decreases as a result of chemistry. The POA essentially boils away as the vapors are consumed.

3 Results and discussion

3.1 Typical experiment and PMF analysis

Figure 1a shows the time series for experiment LEV1-5.2. The data are not corrected for the loss of particles to the chamber walls. This was a typical experiment with POA present in the chamber after filling with diluted exhaust. Figure S.2 in the Supplement shows a similar time series for an experiment without POA in the chamber ("pure SOA", LEV2-1.2).

The experiments consist of four phases: (I) introduction of diluted exhaust into the clean chamber over the course of the UC, (II) characterization of the primary emissions in the chamber ($\sim$ 0.5–1 h), (III) photo-oxidation ($\sim$ 3 h), and (IV) characterization of aged aerosol in the dark ($\sim$ 1 h). For experiment LEV1-5.2 shown in Fig. 1, chamber filling began at $t = -1.39$ h and finished at $t = -.74$ h. The POA was then characterized for approximately 45 min in the dark chamber while HONO and propene were added to the chamber. Modulations in the aerosol concentration for $-1<t<0$ indicate periods when the sample was passed through a thermodenuder (An et al., 2007). Photo-oxidation was initiated at $t = 0$. In this experiment SOA formation was prompt, and the measured OA concentration increased from ~ 1 to $\sim 4\,\mu g\,m^{-3}$ in 1.5 h.

Figure 1a also shows the results of a two-factor PMF solution with FPEAK = 0. The two-factor solution yields distinct POA and SOA factors. The temporal split between the two factors is "clean"; i.e., the concentration of the SOA factor is essentially zero

ACPD
13, 24263–24300, 2013

($< 0.3\,\mu g\,m^{-3}$) for the entire chamber filling and primary characterization period ($t<0$) of the experiment. This is expected based on the design of the experiment. By definition, the SOA concentration is strictly zero for $t<0$, and the PMF solution captures this fact. The concentration of the SOA factor increases dramatically with the onset of photo-oxidation, peaking at approximately $3.5\,\mu g\,m^{-3}$.

After initially spiking when dilute exhaust was first added to the chamber ($t = -1.65$), the concentration of the POA factor decreased because of wall losses and dilution during chamber filling. The concentration of the POA factor continued to decrease during the photo-oxidation portion of the experiment because of wall losses.

In many chamber experiments, SOA is calculated as the difference between the observed OA mass concentration and the assumed concentration of conserved (i.e., non-evaporating) seed particles. The seed particles are assumed to undergo first-order loss to the chamber walls, and the wall loss rate constant (k_{wall}) can be constrained by tracers such as black carbon or particulate sulfate (Hildebrandt et al., 2009; Grieshop et al., 2009b; Hennigan et al., 2011). In experiments where POA is present, it is typically assumed to be a conserved tracer, and the SOA concentration is therefore the difference between the measured total OA and the calculated POA concentrations (Weitkamp et al., 2007).

The dashed blue line in Fig. 1a shows the POA concentration for $t > -0.75$ h (after filling was complete) assuming first-order wall loss. The wall loss rate was determined from black carbon decay. The traditional definition of POA (blue line) and the PMF-derived POA factor have a similar time trend, suggesting that for this experiment, the traditional method of determining the split between POA and SOA is robust. The POA/SOA split is explored in further detail in Sect. 3.3.

The residual of the two-factor PMF solution is shown in Fig. 1b. The absolute value of the residual is less than $0.4\,\mu g\,m^{-3}$ (Σresidual/ΣOA < 0.2) with the exception of several data points when the aerosol was sampled through the thermodenuder. The two-factor solution is relatively insensitive to FPEAK. Varying FPEAK between −1 and 1 did not

ACPD
13, 24263–24300, 2013

have a significant impact on the magnitude of the residual, the ratio Σresidual/ΣOA, or the mass spectra or time series of the two factors.

The PMF solution is limited by the accuracy of the quadrupole AMS used in this study. The lower quantifiable limit for OA concentration with this AMS is 0.3–0.5 $\mu g\,m^{-3}$; in fact, scans taken with a HEPA filter directly upstream of the inlet routinely measure organic aerosol concentrations of 0.3 $\mu g\,m^{-3}$. Thus, this particular AMS is unable to determine absolute concentrations less than 0.3 $\mu g\,m^{-3}$ for the 2.5 min sample averaging time used here. By extension the concentrations of PMF factors smaller than this threshold, such as the SOA factor for $t<0$, are effectively zero.

Adding a third or fourth factor does not improve the performance of the PMF solution. The residual for the three-factor solution is nearly identical to the two-factor solution. Adding additional factors does not substantially improve $Q/Q_{expected}$. For the case shown in Fig. 1, the addition of a third factor reduces $Q/Q_{expected}$ by 7 %. Additionally, the concentration of the third factor is nearly constant with time, and is associated with neither the addition of dilute exhaust to the chamber nor photo-oxidation, and therefore is not physically interpretable.

Figure 2 shows the mass spectra of the POA and SOA factors for the experiment shown in Fig. 1. The POA mass spectrum is indicative of a large contribution of reduced (C_xH_y) hydrocarbon species. m/z 43 (f_{43} = 0.104) is the most abundant ion in the mass spectrum, and the series of C_nH_{2n+1} (m/z 43, 57, etc.) and C_nH_{2n-1} (m/z 41, 55, etc.) are evident. There is a high correlation between the POA mass spectrum and the HOA factor derived from ambient datasets (R^2 = 0.98; Fig. 2c) (Zhang et al., 2005). There is also a high correlation between the POA factor and the diesel POA for vehicle D5 (e.g., Fig. 4f).

The mass spectrum of the SOA factor in Fig. 2a indicates substantial oxygen. m/z 44 (f_{44} = 0.103) is the largest peak in the mass spectrum, consistent with significant oxidation. Reduced peaks such as m/z 57 are depleted (f_{57} = 0). Given its relatively short photochemical age, one would expect the SOA factor to be most similar to ambient SV-OOA. However, the SOA factor does not have a high correlation with published

ACPD
13, 24263–24300, 2013

spectra for ambient or laboratory OA. Figure 2d shows the comparison between the SOA factor and the average SV-OOA factor from Ng et al. (2011b) and indicates a weak correlation between the two spectra. Similarly poor correlations were observed between the SOA factor and an average LV-OOA mass spectrum (Ng et al., 2011b) (e.g., Fig. 4h) as well as the mass spectrum for *m*-xylene SOA (Bahreini et al., 2005).

Strong correlations between the mass spectra for the SOA factor and ambient OOA factors or published SOA mass spectra are not necessarily expected, whereas the high correlation between the mass spectra of the POA factor and published HOA are expected. Ambient HOA is thought to be dominated by fresh combustion emissions, especially from internal combustion engines, and therefore should have a mass spectrum similar to the POA observed here. The OOA factors, which represent ambient SOA, are a combination of SOA from many sources, including dilute exhaust, biogenic emissions, and other sources. Similarly, while *m*-xylene is a component of gasoline and gasoline vehicle exhaust, there is no indication that it is the primary SOA-forming species in dilute engine exhaust (Gordon et al., 2013a, b; Odum et al., 1997).

Table 1 lists each of the experiments considered here, and indicates whether or not PMF was used to deconvolve the AMS data (i.e., whether or not POA was present in the chamber after filling). Eight of the experiments listed in Table 1 did not require PMF. Seven of these experiments were "pure SOA" experiments where no POA was present. One experiment (LEV1-6.3) had POA present, but no SOA was formed. The lack of SOA formation in this experiment was confirmed both by wall-loss based mass analysis and by PMF. For experiments that used PMF, Table 1 also indicates the number of factors used in the solution. Seven of the eight experiments that required PMF analysis used a two-factor solution with distinct POA and SOA factors, such as the case described above for experiment LEV1-5.2.

For one experiment (LEV1-6.1), a third PMF factor was required. A high nitrate SOA factor ($f_{30} = 0.48$, Fig. S.3) appeared immediately after the onset of photo-oxidation. The nitrate SOA factor contributed > 50 % of the SOA mass for the first hour of photo-oxidation, but was quickly eclipsed by a more typical SOA factor, with a mass spectrum

ACPD
13, 24263–24300, 2013

similar to Fig. 2a, for t>1.5 h. By the end of the photo-oxidation portion of the experiment, the nitrate SOA factor contributed ~20 % of the suspended SOA mass. The discussion of experiment LEV1-6.1 below considers only the POA and non-nitrate SOA factors.

Craven et al. (2012) recently conducted PMF analysis of SOA generated in a smog chamber from the photo-oxidation of *n*-dodecane (Craven et al., 2012). They determined three SOA factors: an initial SOA formed at the onset of photo-oxidation, and two progressively more oxidized SOA factors that appeared at t>5 and t>10 h, respectively. The number of PMF factors determined by Craven et al. is broadly consistent with the PMF analysis presented here. Specifically, for 14 of the 16 experiments, we identify a single SOA that is present either in "pure" form (no PMF) or as a single PMF SOA factor. We terminated oxidation after t = 3 h, and observed similar OH radical concentrations (and integrated OH exposures) as Craven et al. over the same time period (Craven et al., 2012; Gordon et al., 2013a, b). Thus, it is reasonable to expect that second and third generation SOA factors such as those observed by Craven et al. would not be observed in these experiments, but could be observed at longer timescales (and additional photo-oxidation). The presence of a single SOA factor in this study is also indication that these experiments probe the first generation of oxidation chemistry.

The presence of a single SOA mass spectrum is in contrast to the results of Sage et al. (2008). Using exhaust from a diesel engine and the residual method to determine the SOA mass spectrum, Sage et al. (2008) observed that the SOA mass spectrum continuously changed over the entire 5 h photo-oxidation period of their experiment. Furthermore, the SOA formed early (t<2.25 h) by Sage et al. (2008) had a higher abundance of m/z 43 than 44, whereas the SOA factor identified in Fig. 2a has a 43/44 ratio of 0.37. The reasons for the differences between the static SOA factor determined here and the evolving SOA observed in Sage et al are unclear. One possibility is different chemical mechanisms between gasoline and diesel engine exhaust, however that seems unlikely as PMF analysis of the diesel experiments considered here also generated a single SOA factor. Another explanation might be the apportionment

ACPD
13, 24263–24300, 2013

of all OA mass at m/z 57 to POA in the residual method. As noted above, this assumption might lead to an erroneous split between POA and SOA mass, which has a direct impact on the calculated SOA and POA mass spectra.

3.2 Mass spectra of PMF factors

3.2.1 Gasoline vehicles

Figure 3a and b show triangle plots (Ng et al., 2010, 2011a), plots of f_{43} versus f_{44}, for the gasoline and diesel vehicles. The POA for three of the four gasoline experiments (open symbols in Fig. 3a) cluster in an area near $f_{43} = 0.1$ and $f_{44}<0.05$. The POA in each of these cases is highly correlated with the ambient HOA factor (e.g., Figs. 2c and 4f) (Zhang et al., 2005). The POA mass spectrum for experiment LEV1-6.2 is more oxidized. It has a higher abundance of m/z 44 ($f_{44} = 0.047$) and a lower abundance of m/z 43 than either the ambient HOA factor or the POA factors from the other gasoline vehicles. The reason for this is not clear, as the POA from the other two experiments with the same vehicle (LEV1-6.1, LEV1-6.3) did not exhibit high f_{44}. In general, vehicle LEV1-6 was classified as a "high emitter" and had difficulties with its emissions control system. This vehicle also had the greatest experiment-to-experiment variability of fuel economy, PM, and NO_x emissions of any of the vehicles in the test fleet (May et al., 2013c). The POA from experiment LEV1-6.2 may be another manifestation of this variability.

The SOA from the "pure-SOA" gasoline-powered vehicles are shown as diamonds with black borders in Fig. 3a. There is remarkable consistency in both f_{43} (0.06–0.07) and f_{44} (0.1–0.14, with most vehicles between 0.12–0.14) for these vehicles, independent of control technology (LEV-1 versus LEV-2). The total, wall-loss-corrected amount of SOA formed in these experiments was also consistent from vehicle to vehicle ($9.6 \pm 2.9\,\mu g\,m^{-3}$).

The composition of SOA from the "pure SOA" experiments does not develop or age with photo-oxidation. Figure S.4 in the Supplement shows time series of f_{44} and f_{43} for

ACPD
13, 24263–24300, 2013

the "pure SOA" experiments. In each case, with the possible exception of a handful of data points immediately after the onset of photo-oxidation, f_{43} andf_{44} are both constant. This suggests that the same SOA precursors are sampled throughout the experiment, and that these precursors are not completely consumed. Thus these experiments sample primarily the first generation of oxidation chemistry.

The SOA factors for gasoline vehicles determined from PMF analysis are shown as solid symbols with no border in Fig. 3a. The SOA factors for these three experiments have lower f_{43} than the "pure SOA" experiments, and a similar range of f_{44}. It is noted above that the SOA factor for experiment LEV1-5.2 (Fig. 2) is poorly correlated with an average ambient SV-OOA factor. This poor correlation extends to the entire gasoline fleet tested – the SOA simply does not look like SV-OOA. Similarly, the average SOA composition for the gasoline vehicles has a weak correlation – a high R^2 but a slope significantly less than unity – with ambient LV-OOA (Fig. 4h).

The blue dashed line in Figure 3a is a linear fit to the data in f_{43} versus f_{44} space. If OA progresses from POA along the linear fit towards SOA, the line provides a rough trajectory of changes in OA composition with photochemical aging. This line is used, along with the relationships of f_{44} to O : C (Aiken et al., 2008) and f_{43} to H : C (Ng et al., 2011a), to translate the data from Fig. 3a into a van Krevelen plot in Fig. 3c. When translated to van Krevelen space, the gasoline experiments fall along a line with a slope of −0.68. This suggests that SOA formation chemistry in these experiments is a combination of carboxylic acid and alcohol/peroxide formation (Ng et al., 2011a; Heald et al., 2010).

The van Krevelen slope of −0.68 is similar to that reported by Ng et al. for ambient data (Ng et al., 2011a). It is also similar to the range of slopes observed by Lambe et al. (2012) for the photo-oxidation of n-alkanes, diesel fuel, and crude oil in a flow tube reactor. Heald et al. (2010) reported a slightly higher slope of approximately −1 for ambient data. Overall, the van Krevelen plot suggests that the SOA chemistry observed in the gasoline vehicle smog chamber experiments is atmospherically relevant.

ACPD
13, 24263–24300, 2013

3.2.2 Diesel vehicles

Figure 3b shows the triangle plot for POA and SOA factors for the two diesel vehicles. We focus first on vehicle D5, which is from model year 2001 and does not have any exhaust aftertreatment. The POA from vehicle D5 (open diamonds) clusters around $f_{43} = 0.08$, $f_{44} = 0.03$. Figure 4b shows the full mass spectrum for the POA, which has a high correlation with the ambient HOA factor (Fig. 4d) and the average gasoline POA factor (Fig. 4f). The mass spectrum has high abundances of the C_nH_{2n+1} and C_nH_{2n-1} series of ions.

Vehicle D4 was a 2005 model year vehicle equipped with a diesel oxidation catalyst (DOC). The mass spectrum for the POA from vehicle D5 is shown in Fig. 4a. It has both a high abundance of m/z 44 ($f_{44} = 0.1$) and the characteristic C_nH_{2n+1} and C_nH_{2n-1} series of ions typical of HOA. With the exception of the high f_{44} (and f_{18}, which is set equal to f_{44} in the fragmentation table), the mass spectra of the POA from D4 and D5 are highly correlated (Fig. 4c). Chirico et al observed similar POA from a DOC-equipped passenger car (Chirico et al., 2010). Specifically, they reported elevated abundances of oxygen-containing ions superimposed on top of a typical diesel POA backbone.

The differences between the POA mass spectrum for vehicle D4 and the ambient HOA factor suggests that vehicles without DOC dominate the on-road diesel fleet. This is indeed the case. Equipping a large fraction of the diesel fleet with DOC might therefore change the canonical spectrum of ambient HOA to include more oxygenated ions.

Figure 4c–h offers several comparisons of the gasoline and diesel POA and SOA. The mass spectra of the POA emitted by the uncontrolled diesel vehicle (D5) and the gasoline automobiles are highly correlated with both each other and with the ambient HOA mass spectrum. The SOA formed from the gasoline and diesel vehicles is also similar. This is evident from both the triangle plots in Fig. 3 and the scatter plot in Fig. 4g. The similarity between gasoline and diesel exhaust SOA is interesting because the emissions of SOA precursors from the two types of engines are different, with diesel

ACPD
13, 24263–24300, 2013

engines having a lower emission rate of SOA precursors, but also emitting compounds of lower volatility (May et al., 2013c; Schauer et al., 1999, 2002).

The black dashed line in Figure 3b is a linear fit to the diesel POA and SOA data in f_{43} versus f_{44} space. As with the gasoline case, we make the assumption that OA progresses from POA along the linear fit towards SOA. This line is translated into van Krevelen space in Fig. 3c. In this context, the diesel experiments presented here fall along a line with a slope of −0.43. As with the gasoline vehicles, the van Krevelen slope for the diesel vehicles suggests that SOA formation chemistry in these experiments is a combination of carboxylic acid and alcohol/peroxide formation (Ng et al., 2011a; Heald et al., 2010).

3.3 Temporal behavior of POA factors

Section 3.1 noted that the traditional definition of SOA – i.e., assuming that POA was lost to the chamber walls with first order kinetics – produced a reasonable SOA/POA split for the experiment shown in Fig. 1. Figure 5 shows two more cases, experiments with vehicles D4 and D5. The data are not corrected for particle losses to the chamber walls. The blue line in each panel shows a first order wall loss rate as determined from measured BC concentrations.

In experiment D5.2 (Fig. 5a), the POA factor follows the first-order wall loss rate for the entire experiment. This is consistent with the typical treatment of POA in these sort of dilute exhaust smog chamber experiments, (Hennigan et al., 2011; Miracolo et al., 2011, 2012; Robinson et al., 2007; Weitkamp et al., 2007) and in this experiment gives an accurate estimate for the SOA mass formed during photo-oxidation. The POA for the gasoline vehicles tested here also followed the expected first-order decay curve.

The POA for vehicle D4 exhibited behavior that was unique among the vehicles tested here (Fig. 5b). Before the start of photo-oxidation ($t<0$), the POA followed a first-order wall loss rate. After the start of photo-oxidation at $t = 0$, the POA evaporated, and disappeared completely within one hour. This rapid POA loss was observed in both experiments with vehicle D4. For this vehicle, assuming that the POA follows a first or-

ACPD
13, 24263–24300, 2013

der loss rate overestimates the POA concentration, and therefore underestimates the SOA formation.

The opposite behavior can also be observed. In experiments with a gas-turbine engine, Miracolo et al. (2012) observed very large concentrations of SOA (> 100 μg m^{-3}) during photo-oxidation. In such cases, PMF analysis indicates that the POA concentration increases (Fig. S.5). This is likely a result of gas-particle partitioning driving primary vapors into the particle phase at high C_{OA} (Donahue et al., 2006; Pankow, 1994). When partitioning causes the POA concentration to increase, the first-order wall loss assumption underestimates the POA concentration, and subsequently overestimates the formation of SOA.

The cases presented here are not sufficient to definitively comment on the standard assumption that POA behaves as a conserved tracer. For nearly all of the vehicles presented here it seems to be a good assumption, but it is a very poor assumption for vehicle D4. Ultimately the POA time series needs to be evaluated on a case-by-case basis.

The time series of the POA factor can also be used to inform the mixing behavior of POA and SOA in these experiments. A basis set model is used to investigate POA/SOA mixing in Fig. 6 for vehicle D5. This is the same vehicle as shown in Fig. 5a, where the POA factor decays according to the first-order wall loss rate. The implication of the POA factor decaying at the first-order loss rate in Fig. 5a is that the wall-loss corrected concentration of the POA factor in Fig. 6 should be essentially constant. This is more-or-less the case. The wall-loss corrected concentration of the POA factor (black circles) is 4.6 ± 0.6 μg m^{-3} for t<0 and increases by approximately 1 μg m^{-3} during the first hour of oxidation. For t>1 h, the wall-loss corrected concentration of the POA factor decays slightly.

Figure 6 also shows model results for Cases 1 (blue line) and 2 (red line), as well as Case 2 (black dashed line) with chemistry turned off (k_{OH} = 0). None of the model cases match the POA data perfectly, but Case 1 performs the best. The no-chemistry case is used to investigate the effects of the increase in chamber temperature on partitioning

ACPD
13, 24263–24300, 2013

of the POA. It shows that the ~5 °C increase in chamber temperature would induce roughly 1 μg m^{-3} of POA to evaporate. Case 2 predicts an even greater loss of POA mass, approximately 2.5 μg m^{-3} (50 % of the initial POA), due to gas-phase chemistry removing the vapors that equilibrate with the POA.

Case 1, which assumes ideal mixing between the POA and SOA and no mass transfer limitations for POA evaporation, predicts a roughly constant concentration of POA for the first two hours of oxidation. This occurs because the loss of POA induced by the temperature increase is almost perfectly offset by the increase in C_{OA} from SOA formation (not shown in Fig. 6). Indeed, SOA formation dominates the OA for t>0, increasing from zero concentration at t = 0 to approximately 6 μg m^{-3} at t = 2 h. Case 1 also predicts a slight uptick in the wall-loss corrected POA concentration of ~0.5 μg m^{-3} immediately after the start of photo-oxidation at t = 0. However, this increase is fleeting, and does not match the size or extent of the observed increase in the concentration of the POA factor.

For the data in Fig. 6, we conclude that the observed behavior of the POA is consistent with the POA and SOA forming an ideal mixture, and with prompt equilibration of the OA with the surrounding vapors. Performing the same modeling exercise with the data for the gasoline vehicles reveals that those experiments are also consistent with POA and SOA mixing.

This simple basis set model is not able to predict the rapid POA evaporation for vehicle D4 using either Case 1 or Case 2. Possibilities for why the model fails to predict the extent of POA evaporation in this experiment include either k_{OH} or [OH] could be too low or errors in the estimates for the enthalpy of vaporization (higher ΔH_{vap} would make the POA more sensitive to variations in temperature). However, these parameters have been successfully applied to the other experiments considered here (e.g., Fig. 6), so it seems unlikely that different values for k_{OH} and ΔH_{vap} would be needed for vehicle D4. More experiments exhibiting rapid POA evaporation and/or more rigorous modeling of the smog chamber are likely required to understand the rapid POA evaporation for this vehicle.

ACPD
13, 24263–24300, 2013

4 Conclusions

In this work, we present AMS analysis of OA from smog chamber experiments using dilute exhaust from gasoline and diesel vehicles. The experiments presented here capture approximately 2–5 h of photo-oxidation under ambient OH concentrations. PMF is used to deconvolve POA and SOA factors when substantial POA is present in the dilute exhaust. The results presented here indicate that the observed data can be explained by the formation of a single type of SOA. With one exception, a 2-factor solution with one POA factor and one SOA factor could explain the data when POA was present in the chamber prior to photo-oxidation. "Pure SOA" experiments (no POA present) also produced a single SOA with time-invariant composition.

POA factors determined from PMF analysis are similar to the HOA factor derived from ambient datasets, and contain high abundances of the C_nH_{2n+1} and C_nH_{2n-1} series of ions (Ng et al., 2010, 2011a). Vehicle D4 is the exception. The POA from this vehicle has a high f_{44}, though the C_nH_{2n+1} and C_nH_{2n-1} ions are still present. SOA factors determined from PMF and SOA mass spectra from pure SOA experiments cluster in an area of high f_{44} (~ 0.1) and low f_{43} (~ 0.05). The SOA factors from gasoline and diesel experiments are similar to each other, however the mass spectra of the SOA factors are not similar to published mass spectra of ambient OOA factors (SV-OOA or LV-OOA) or published mass spectra of SOA formed from traditional SOA precursors such as single ring aromatic compounds. The maximum O : C ratio observed here is approximately 0.6, consistent with less-oxidized SV-OOA (Ng et al., 2010, 2011a). Further oxidative processing is required to produce more oxidized LV-OOA (Ng et al., 2010, 2011a; Lambe et al., 2011).

Translation of the AMS data into van Krevelen space (Fig. 3) provides information concerning the oxidation chemistry in these experiments. The slopes for gasoline and diesel exhaust oxidation in van Krevelen space are −0.68 and −0.43. This suggests that SOA formation chemistry is a combination of carboxylic acid and alcohol/peroxide formation (Ng et al., 2011a; Heald et al., 2010) and is an indication that the photo-

ACPD
13, 24263–24300, 2013

oxidation chemistry in the experiments presented here is atmospherically relevant. Ambient OA data, when plotted in van Krevelen space, exhibits slopes between −1 (Heald et al., 2010), indicative of chemistry dominated by carboxylic acid formation, and −0.5 (Ng et al., 2011a), indicative of chemistry dominated by a mixture of acid formation and alcohol/peroxide formation.

A simple basis set model was used to interpret the time evolution of the POA and SOA factors (Fig. 6). For all of the experiments except for those using vehicle D4, a model assuming ideal mixing between POA and SOA produces better agreement with the data than a version of the model that assumes the POA and SOA form distinct phases. Neither version of the model is able to describe the rapid and complete evaporation of the POA for vehicle D4. We therefore conclude that the POA and SOA are mixing in these experiments.

Supplementary material related to this article is available online at http://www.atmos-chem-phys-discuss.net/13/24263/2013/acpd-13-24263-2013-supplement.pdf.

Acknowledgements. We thank Matti Maricq at Ford and Hector Maldonado at the California Air Resource Board for helping organize and lead the Linking Tailpipe-to-Ambient project. This research would not have been possible without the hard work of the excellent and dedicated staff at the California Air Resources Board Haagen-Smit Laboratory. Funding was provided by the U.S. Environmental Protection Agency National Center for Environmental Research (NCER) through the STAR program (R833748) and the Coordinating Research Council through A74/E96. The California Air Resources Board provided significant in-kind support, including vehicle recruitment, vehicle testing, and sample analysis. The views, opinions, and/or findings contained in this paper are those of the authors and should not be construed as an official position of the funding agencies.

ACPD
13, 24263–24300, 2013

References

Aiken, A. C., DeCarlo, P. F., Kroll, J. H., Worsnop, D. R., Huffman, J. A., Docherty, K. S., Ulbrich, I. M., Mohr, C., Kimmel, J. R., Sueper, D., Sun, Y., Zhang, Q., Trimborn, A., Northway, M., Ziemann, P. J., Canagaratna, M. R., Onasch, T. B., Alfarra, M. R., Prevot, A. S. H., Dommen, J., Duplissy, J., Metzger, A., Baltensperger, U., and Jimenez, J. L.: O/C and OM/OC ratios of primary, secondary, and ambient organic aerosols with high-resolution time-of-flight aerosol mass spectrometry, Environ. Sci. Technol., 42, 4478–4485, 2008.

Aiken, A. C., Salcedo, D., Cubison, M. J., Huffman, J. A., DeCarlo, P. F., Ulbrich, I. M., Docherty, K. S., Sueper, D., Kimmel, J. R., Worsnop, D. R., Trimborn, A., Northway, M., Stone, E. A., Schauer, J. J., Volkamer, R. M., Fortner, E., de Foy, B., Wang, J., Laskin, A., Shutthanandan, V., Zheng, J., Zhang, R., Gaffney, J., Marley, N. A., Paredes-Miranda, G., Arnott, W. P., Molina, L. T., Sosa, G., and Jimenez, J. L.: Mexico City aerosol analysis during MILAGRO using high resolution aerosol mass spectrometry at the urban supersite (T0) – Part 1: Fine particle composition and organic source apportionment, Atmos. Chem. Phys., 9, 6633–6653, doi:10.5194/acp-9-6633-2009, 2009.

Allan, J. D., Delia, A. E., Coe, H., Bower, K. N., Alfarra, M. R., Jimenez, J. L., Middlebrook, A. M., Drewnick, F., Onasch, T. B., and Canagaratna, M. R.: A generalised method for the extraction of chemically resolved mass spectra from aerodyne aerosol mass spectrometer data, J. Aerosol Sci., 35, 909–922, 2004.

An, W. J., Pathak, R. K., Lee, B.-H., and Pandis, S. N.: Aerosol volatility measurement using an improved thermodenuder: Application to secondary organic aerosol, J. Aerosol Sci., 38, 305–314, 2007.

Asa-Awuku, A., Miracolo, M. A., Kroll, J. H., Robinson, A. L., and Donahue, N. M.: Mixing and phase partiitioning of primary and secondary organic aerosols, Geophys. Res. Lett., 36, L15827, doi:10.1029/2009GL039301, 2009.

Atkinson, R. and Arey, J.: Atmospheric degradation of volatile organic compounds, Chem. Rev., 103, 4605–4638, 2003.

Bahreini, R., Keywood, M. D., Ng, N. L., Varutbangkul, V., Gao, S., Flagan, R. C., Seinfeld, J. H., Worsnop, D. R., and Jimenez, J. L.: Measurement of secondary organic aerosol from oxidation of cycloalkanes, terpenes, and m-xylene using an aerodyne aerosol mass spectrometer, Environ. Sci. Technol., 39, 5674–5688, doi:10.1021/es048061a, 2005.

ACPD
13, 24263–24300, 2013

Canagaratna, M. R., Jayne, J. T., Ghertner, D. A., Herndon, S., Shi, Q., Jimenez, J. L., Silva, P. J., Williams, P., Lanni, T., Drewnick, F., Demerjian, K. L., Kolb, C. E., and Worsnop, D. R.: Chase studies of particulate emissions from in-use New York City vehicles, Aerosol Sci. Technol., 38, 555–573, 2004.

Canagaratna, M. R., Jayne, J. T., Jimenez, J. L., Allan, J. D., Alfarra, M. R., Zhang, Q., Onasch, T. B., Drewnick, F., Coe, H., Middlebrook, A., Delia, A., Williams, L. R., Trimborn, A. M., Northway, M. J., DeCarlo, P. F., Kold, C. E., Davidovits, P., and Worsnop, D. R.: Chemical and microphysical characterization of ambient aerosols with the aerodyne aerosol mass spectrometer, Mass Spectrom. Rev., 26, 185–222, 2007.

Chirico, R., DeCarlo, P. F., Heringa, M. F., Tritscher, T., Richter, R., Prévôt, A. S. H., Dommen, J., Weingartner, E., Wehrle, G., Gysel, M., Laborde, M., and Baltensperger, U.: Impact of aftertreatment devices on primary emissions and secondary organic aerosol formation potential from in-use diesel vehicles: results from smog chamber experiments, Atmos. Chem. Phys., 10, 11545–11563, doi:10.5194/acp-10-11545-2010, 2010.

Craven, J. S., Yee, L. D., Ng, N. L., Canagaratna, M. R., Loza, C. L., Schilling, K. A., Yatavelli, R. L. N., Thornton, J. A., Ziemann, P. J., Flagan, R. C., and Seinfeld, J. H.: Analysis of secondary organic aerosol formation and aging using positive matrix factorization of high-resolution aerosol mass spectra: application to the dodecane low-NO_x system, Atmos. Chem. Phys., 12, 11795–11817, doi:10.5194/acp-12-11795-2012, 2012.

Docherty, K. S., Stone, E. A., Ulbrich, I. M., DeCarlo, P. F., Snyder, D. C., Schauer, J. J., Peltier, R. E., Weber, R. J., Murphy, S. M., Seinfeld, J. H., Grover, B. D., Eatough, D. J., and Jimenez, J. L.: Apportionment of primary and secondary organic aerosols in sourthern california during the 2005 Study of Organic Aerosols in Riverside (SOAR-1), Environ. Sci. Technol., 42, 7655–7662, 2008.

Donahue, N. M., Robinson, A. L., Stanier, C. O., and Pandis, S. N.: Coupled partitioning, dilution, and chemical aging of semivolatile organics, Environ. Sci. Technol., 40, 2635–2643, 2006.

Donahue, N. M., Robinson, A. L., and Pandis, S. N.: Atmospheric organic particulate matter: From smoke to secondary organic aerosol, Atmos. Environ., 43, 94–106, 2009.

Donahue, N. M., Epstein, S. A., Pandis, S. N., and Robinson, A. L.: A two-dimensional volatility basis set: 1. organic-aerosol mixing thermodynamics, Atmos. Chem. Phys., 11, 3303–3318, doi:10.5194/acp-11-3303-2011, 2011.

ACPD
13, 24263–24300, 2013

Donahue, N. M., Kroll, J. H., Pandis, S. N., and Robinson, A. L.: A two-dimensional volatility basis set – Part 2: Diagnostics of organic-aerosol evolution, Atmos. Chem. Phys., 12, 615–634, doi:10.5194/acp-12-615-2012, 2012.

Farmer, D. K., Matsunaga, A., Docherty, K. S., Surratt, J. D., Seinfeld, J. H., Ziemann, P. J., and Jimenez, J. L.: Response of an aerosol mass spectrometer to organonitrates and organosulfates and implications for atmospheric chemistry, P. Natl. Acad. Sci., 107, 6670–6675, 2010.

Gordon, T. D., Presto, A. A., Nguyen, N. T., Robertson, W. H., Na, K., Sahay, K. N., Zhang, M., Maddox, C., Rieger, P., Chattopadhyay, S., Maldonado, H., Maricq, M. M., and Robinson, A. L.: Secondary organic aerosol production from diesel vehicle exhaust: impact of aftertreatment, fuel chemistry and driving cycle, Atmos. Chem. Phys. Discuss., in press, 2013a.

Gordon, T. D., Presto, A. A., May, A. A., Nguyen, N. T., Lipsky, E. M., Donahue, N. M., Gutierrez, A., Zhang, M., Maddox, C., Rieger, P., Chattopadhyay, S., Maldonado, H., Maricq, M. M., and Robinson, A. L.: Secondary organic aerosol formation exceeds primary particulate matter emissions for light-duty gasoline vehicles, Atmos. Chem. Phys. Discuss., 13, 23173–23216, doi:10.5194/acpd-13-23173-2013, 2013.

Grieshop, A. P., Donahue, N. M., and Robinson, A. L.: Laboratory investigation of photochemical oxidation of organic aerosol from wood fires 2: analysis of aerosol mass spectrometer data, Atmos. Chem. Phys., 9, 2227–2240, doi:10.5194/acp-9-2227-2009, 2009a.

Grieshop, A. P., Logue, J. M., Donahue, N. M., and Robinson, A. L.: Laboratory investigation of photochemical oxidation of organic aerosol from wood fires 1: measurement and simulation of organic aerosol evolution, Atmos. Chem. Phys., 9, 1263–1277, doi:10.5194/acp-9-1263-2009, 2009b.

Heald, C. L., Kroll, J. H., Jimenez, J. L., Docherty, K. S., DeCarlo, P. F., Aiken, A. C., Chen, Q., Martin, S. T., Farmer, D. K., and Artaxo, P.: A simplified description of the evolution of organic aerosol compositoin in the atmosphere, Geophys. Res. Lett., 37, L08803, doi:10.1029/2010GL042737, 2010.

Hennigan, C. J., Miracolo, M. A., Engelhart, G. J., May, A. A., Presto, A. A., Lee, T., Sullivan, A. P., McMeeking, G. R., Coe, H., Wold, C. E., Hao, W.-M., Gilman, J. B., Kuster, W. C., de Gouw, J., Schichtel, B. A., J. L. Collett Jr., Kreidenweis, S. M., and Robinson, A. L.: Chemical and physical transformations of organic aerosol from the photo-oxidation of open biomass burning emissions in an environmental chamber, Atmos. Chem. Phys., 11, 7669–7686, doi:10.5194/acp-11-7669-2011, 2011.

ACPD
13, 24263–24300, 2013

Heringa, M. F., DeCarlo, P. F., Chirico, R., Tritscher, T., Dommen, J., Weingartner, E., Richter, R., Wehrle, G., Prevot, A. S. H., and Baltensperger, U.: Investigations of primary and secondary particulate matter of different wood combustion appliances with a high-resolution time-of-flight aerosol mass spectrometer, Atmos. Chem. Phys., 11, 5945–5957, 10, http://www.atmos-chem-phys.net/11/5945/10/.5194/acp-11-5945-2011, 2012.

Hildebrandt, L., Donahue, N. M., and Pandis, S. N.: High formation of secondary organic aerosol from the photo-oxidation of toluene, Atmos. Chem. Phys., 9, 2973–2986, doi:10.5194/acp-9-2973-2009, 2009.

Huffman, J. A., Docherty, K. S., Aiken, A. C., Cubison, M. J., Ulbrich, I. M., DeCarlo, P. F., Sueper, D., Jayne, J. T., Worsnop, D. R., Ziemann, P. J., and Jimenez, J. L.: Chemically-resolved aerosol volatility measurements from two megacity field studies, Atmos. Chem. Phys., 9, 7161–7182, doi:10.5194/acp-9-7161-2009, 2009.

Jayne, J. T., Leard, D. C., Zhang, X. F., Davidovits, P., Smith, K. A., Kolb, C. E., and Worsnop, D. R.: Development of an aerosol mass spectrometer for size and composition analysis of submicron particles, Aerosol Sci. Technol., 33, 49–70, 2000.

Kanakidou, M., Seinfeld, J. H., Pandis, S. N., Barnes, I., Dentener, F. J., Facchini, M. C., Van Dingenen, R., Ervens, B., Nenes, A., Nielsen, C. J., Swietlicki, E., Putaud, J. P., Balkanski, Y., Fuzzi, S., Horth, J., Moortgat, G. K., Winterhalter, R., Myhre, C. E. L., Tsigaridis, K., Vignati, E., Stephanou, E. G., and Wilson, J.: Organic aerosol and global climate modelling: a review, Atmos. Chem. Phys., 5, 1053–1123, doi:10.5194/acp-5-1053-2005, 2005.

Kroll, J. H., Smith, J. D., Che, D. L., Kessler, S. H., Worsnop, D. R., and Wilson, K. R.: Measurement of fragmentation and functionalization pathways in the heterogeneous oxidation of oxidized organic aerosol, Phys. Chem. Chem. Phys., 11, 8005–8014, 2009.

Lambe, A. T., Onasch, T. B., Massoli, P., Croasdale, D. R., Wright, J. P., Ahern, A. T., Williams, L. R., Worsnop, D. R., Brune, W. H., and Davidovits, P.: Laboratory studies of the chemical composition and cloud condensation nuclei (CCN) activity of secondary organic aerosol (SOA) and oxidized primary organic aerosol (OPOA), Atmos. Chem. Phys., 11, 8913–8928, doi:10.5194/acp-11-8913-2011, 2011.

Lambe, A. T., Onasch, T. B., Croasdale, D. R., Wright, J. P., Martin, A. T., Franklin, J. P., Massoli, P., Kroll, J. H., Canagaratna, M. R., Brune, W. H., Worsnop, D. R., and Davidovits, P.: Transitions from functionalization to fragmentation reactions of laboratory secondary organic aerosol (SOA) generated from the OH oxidation of alkane precursors, Environ. Sci. Technol., 46, 5430–5437, 2012.

ACPD
13, 24263–24300, 2013

Lanz, V. A., Alfarra, M. R., Baltensperger, U., Buchmann, B., Hueglin, C., and Prévôt, A. S. H.: Source apportionment of submicron organic aerosols at an urban site by factor analytical modelling of aerosol mass spectra, Atmos. Chem. Phys., 7, 1503–1522, doi:10.5194/acp-7-1503-2007, 2007.

Massoli, P., Fortner, E. C., Canagaratna, M. R., Williams, L. R., Zhang, Q., Sun, Y., Schwab, J. J., Trimborn, A., Onasch, T. B., Demerjian, K. L., Kolb, C. E., Worsnop, D. R., and Jayne, J. T.: Pollution gradients and chemical characterization of particulate matter from vehicular traffic near major roadways: Results from the 2009 Queens College air quality study in NYC, Aerosol Sci. Technol., 46, 1201–1218, doi:10.1080/02786826.2012.701784, 2012.

May, A. A., Presto, A. A., Gordon, T. D., Nguyen, N. T., Hennigan, C. J., and Robinson, A. L.: Gas-particle partitioning of primary organic aerosol emissions: (2) diesel vehicles, Environ. Sci. Technol., 47, 8288–8296, doi:10.1021/es400782j, 2013a.

May, A. A., Presto, A. A., Nguyen, N. T., Hennigan, C. J., Gordon, T. D., and Robinson, A. L.: Gas-particle partitioning of primary organic aerosol emissions: (1) gasoline vehicle exhaust, Atmos. Environ., 77, 128–139, doi:10.1016/j.atmosenv.2013.04.060, 2013b.

May, A. A., Nguyen, N. T., Presto, A. A., Gordon, T. D., Lipsky, E. M., Karve, M., Guitierrez, A., Robertson, W. H., Zhang, M., Chang, O., Chen, S., Cicero-Fernandez, P. Fuentes, M., Huang, S.-M., Ling, R., Long, J., Maddox, C., Massetti, J., McCauley, E., Na, K., Pang, Y., Rieger, P., Sax, T., Truong, T., Vo, T., Chattopadhyay, S., Maldonado, H., Maricq, M. M., and Robinson, A. L.: Primary gas and PM emissions from light and heavy duty vehicles, Atmos. Environ., submitted, 2013c.

Miracolo, M. A., Presto, A. A., Lambe, A. T., Hennigan, C. J., Donahue, N. M., Kroll, J. H., Worsnop, D. R., and Robinson, A. L.: Secondary organic aerosol formation from low-volatility organic vapors in motor vehicle emissions, Environ. Sci. Technol., 44, 1638–1643, 2010.

Miracolo, M. A., Hennigan, C. J., Ranjan, M., Nguyen, N. T., Gordon, T. D., Lipsky, E. M., Presto, A. A., Donahue, N. M., and Robinson, A. L.: Secondary aerosol formation from photochemical aging of aircraft exhaust in a smog chamber, Atmos. Chem. Phys., 11, 4135–4147, doi:10.5194/acp-11-4135-2011, 2011.

Miracolo, M. A., Drozd, G. T., Jathar, S. H., Presto, A. A., Lipsky, E. M., Corporan, E., and Robinson, A. L.: Fuel composition and secondary organic aerosol formation: Gas-turbine exhaust and alternative aviation fuels, Environ. Sci. Technol., 46, 8493–8501, 2012.

Ng, N. L., Canagaratna, M. R., Zhang, Q., Jimenez, J. L., Tian, J., Ulbrich, I. M., Kroll, J. H., Docherty, K. S., Chhabra, P. S., Bahreini, R., Murphy, S. M., Seinfeld, J. H., Hildebrandt,

ACPD
13, 24263–24300, 2013

L., Donahue, N. M., DeCarlo, P. F., Lanz, V. A., Prévôt, A. S. H., Dinar, E., Rudich, Y., and Worsnop, D. R.: Organic aerosol components observed in Northern Hemispheric datasets from Aerosol Mass Spectrometry, Atmos. Chem. Phys., 10, 4625–4641, doi:10.5194/acp-10-4625-2010, 2010.

Ng, N. L., Canagaratna, M. R., Jimenez, J. L., Chhabra, P. S., Seinfeld, J. H., and Worsnop, D. R.: Changes in organic aerosol composition with aging inferred from aerosol mass spectra, Atmos. Chem. Phys., 11, 6465–6474, doi:10.5194/acp-11-6465-2011, 2011a.

Ng, N. L., Canagaratna, M. R., Jimenez, J. L., Zhang, Q., Ulbrich, I. M., and Worsnop, D. R.: Real-time methods for estimating organic component mass concentrations from aerosol mass spectrometer data, Environ. Sci. Technol., 45, 910–916, doi:10.1021/es102951k, 2011b.

Nordin, E. Z., Eriksson, A. C., Roldin, P., Nilsson, P. T., Carlsson, J. E., Kajos, M. K., Hellén, H., Wittbom, C., Rissler, J., Löndahl, J., Swietlicki, E., Svenningsson, B., Bohgard, M., Kulmala, M., Hallquist, M., and Pagels, J. H.: Secondary organic aerosol formation from idling gasoline passenger vehicle emissions investigated in a smog chamber, Atmos. Chem. Phys., 13, 6101–6116, doi:10.5194/acp-13-6101-2013, 2013.

Odum, J. R., Jungkamp, T. P. W., Griffin, R. J., Flagan, R. C., and Seinfeld, J. H.: The atmospheric aerosol-forming potential of whole gasoline vapor, Science, 276, 96–99, 1997.

Paatero, P.: Least squares formulation of robust non-negative factor analysis, Chemometrics and Intelligent Laboratory Systems, 37, 23–35, 1997.

Paatero, P. and Tapper, U.: Positive matrix factorization: A non-negative factor model with optimal utilization of error estimates of data values, Environmetrics, 5, 111–126, 1994.

Pankow, J. F.: An absorbtion-model gas-particle partitioning of organic compounds in the atmosphere, Atmos. Environ., 28, 185–188, 1994.

Platt, S. M., El Haddad, I., Zardini, A. A., Clairotte, M., Astorga, C., Wolf, R., Slowik, J. G., Temime-Roussel, B., Marchand, N., Ježek, I., Drinovec, L., Mocnik, G., Möhler, O., Richter, R., Barmet, P., Bianchi, F., Baltensperger, U., and Prévôt, A. S. H.: Secondary organic aerosol formation from gasoline vehicle emissions in a new mobile environmental reaction chamber, Atmos. Chem. Phys. Discuss., 12, 28343–28383, doi:10.5194/acpd-12-28343-2012, 2012.

Presto, A. A., Nguyen, N. T., Ranjan, M., Reeder, A. J., Lipsky, E. M., Hennigan, C. J., Miracolo, M. A., Riemer, D. D., and Robinson, A. L.: Fine particle and organic vapor emissions from staged tests of an in-use aircraft engine, Atmos. Environ., 45, 3603–3612, 2011.

ACPD
13, 24263–24300, 2013

Presto, A. A., Hennigan, C. J., Nguyen, N. T., and Robinson, A. L.: Determination of volatility distributions of primary organic aerosol emissions from internal combustion engines using thermal desorption gas chromatography mass spectrometry, Aerosol Sci. Technol., 46, 1129–1139, 2012.

Robinson, A. L., Donahue, N. M., Shrivastava, M. K., Weitkamp, E. A., Sage, A. M., Grieshop, A. P., Lane, T. E., Pierce, J. R., and Pandis, S. N.: Rethinking organic aerosols: Semivolatile emissions and photochemical aging, Science, 315, 1259–1262, doi:10.1126/science.1133061, 2007.

Sage, A. M., Weitkamp, E. A., Robinson, A. L., and Donahue, N. M.: Evolving mass spectra of the oxidized component of organic aerosol: results from aerosol mass spectrometer analyses of aged diesel emissions, Atmos. Chem. Phys., 8, 1139–1152, doi:10.5194/acp-8-1139-2008, 2008.

Samy, S. and Zielinska, B.: Secondary organic aerosol production from modern diesel engine emissions, Atmos. Chem. Phys., 10, 609–625, doi:10.5194/acp-10-609-2010, 2010.

Schauer, J. J., Kleeman, M. J., Cass, G. R., and Simoneit, B. R. T.: Measurement of emissions from air pollution sources. 2. C1 through C30 organic compounds from medium duty diesel trucks, Environ. Sci. Technol., 33, 1578–1587, 1999.

Schauer, J. J., Kleeman, M. J., Cass, G. R., and Simoneit, B. R. T.: Measurement of emissions from air pollution sources. 4. C1 - C32 organic compounds from gasoline-powered motor vehicles, Environ. Sci. Technol., 36, 567–575, 2002.

Song, C., Zaveri, R. A., Alexander, M. L., Thornton, J. A., Madronich, S., Ortega, J. V., Zelenyuk, A., Yu, X. Y., Laskin, A., and Maughan, D. A.: Effect of hydrophobic primary organic aerosols on secondary organic aerosol formation from ozonolysis of alpha-pinene, Geophys. Res. Lett., 34, L20803, doi:10.1029/2007gl030720, 2007.

Song, C., Zaveri, R. A., Shilling, J. E., Alexander, M. L., and Newburn, M.: Effect of hydrophilic organic seed aerosols on secondary organic aerosol formation from ozonolysis of alpha-pinene, Environ. Sci. Technol., 45, 7323–7329, 2011.

Sun, J., Zhang, Q., Canagaratna, M. R., Zhang, Y., Ng, N. L., Sun, Y., Jayne, J. T., Zhang, X., Zhang, X., and Worsnop, D. R.: Highly time- and size-resolved characterization of submicron aerosol particles in Beijing using an Aerodyne aerosol mass spectrometer, Atmos. Environ., 44, 131–140, 2010.

Sun, Y. L., Zhang, Q., Schwab, J. J., Yang, T., Ng, N. L., and Demerjian, K. L.: Factor analysis of combined organic and inorganic aerosol mass spectra from high resolution aerosol

ACPD
13, 24263–24300, 2013

mass spectrometer measurements, Atmos. Chem. Phys., 12, 8537–8551, doi:10.5194/acp-12-8537-2012, 2012.

Ulbrich, I. M., Canagaratna, M. R., Zhang, Q., Worsnop, D. R., and Jimenez, J. L.: Interpretation of organic components from Positive Matrix Factorization of aerosol mass spectrometric data, Atmos. Chem. Phys., 9, 2891–2918, doi:10.5194/acp-9-2891-2009, 2009.

Weitkamp, E. A., Sage, A. M., Donahue, N. M., and Robinson, A. L.: Organic aerosol formation from photochemical oxidation of diesel exhaust in a smog chamber, Environ. Sci. Technol., 41, 6969–6975, 2007.

Zhang, Q., Alfarra, M. R., Worsnop, D. R., Allan, J. D., Coe, H., Canagaratna, M. R., and Jimenez, J. L.: Deconvolution of hydrocarbon-like and oxygenated organic aerosols based on aerosol mass spectrometry, Environ. Sci. Technol., 39, 4938–4952, 2005.

Zhang, Q., Jimenez, J. L., Canagaratna, M. R., Allan, J. D., Coe, H., Ulbrich, I., Alfarra, M. R., Takami, A., Middlebrook, A. M., Sun, Y. L., Dzepina, K., Dunlea, E., Docherty, K., DeCarlo, P. F., Salcedo, D., Onasch, T., Jayne, J. T., Miyoshi, T., Shimono, A., Hatakeyama, S., Takegawa, N., Kondo, Y., Schneider, J., Drewnick, F., Borrmann, S., Weimer, S., Demerjian, K., Williams, P., Bower, K., Bahreini, R., Cottrell, L., Grffin, R. J., Rautiainen, J., Sun, J. Y., Zhang, Y. M., and Worsnop, D. R.: Ubiquity and dominance of oxygenated species in organic aerosols in anthropogenically-influenced northern hemisphere midlatitudes, Geophys. Res. Lett., 34, L13801, doi:10.1029/2007GL029979, 2007.

Zhang, Q., Jimenez, J. L., Canagaratna, M. R., Ulbrich, I. M., Ng, N. L., Worsnop, D. R., and Sun, Y.: Understanding atmospheric organic aerosols via factor analysis of aerosol mass spectrometry: A review, Anal. Bioanal. Chem., 401, 3045–3067, 2011.

ACPD
13, 24263–24300, 2013

Table 1. List of smog chamber experiments. Vehicles are identified by their model year and a unique identifier that indicates either the control level (LEV1 or LEV2) for gasoline vehicles or fuel (D) for diesel vehicles, a number assigned to the vehicle as part of the larger fleet presented in May et al. (2013c), and the experiment number with that particular vehicle.

Test ID	Model year	VOC/NO_x (ppmC ppm^{-1})	SOA produced (μg m^{-3})	PMF	Factors	Notes
LEV1-1.5	1996	3.80	9.29	N	Pure SOA	
LEV2-1.2	2007	3.43	10.7	N	Pure SOA	
LEV1-6.1	2003	3.48	2.39	Y	3	Third factor in PMF is high nitrate SOA component
LEV1-6.2	2003	3.47	8.82	Y	2	
LEV1-6.3	2003	0.25	0	N		No SOA formed, only POA
LEV1-5.2	2000	3.37	3.24	Y	2	
LEV2-1.6	2007	3.28	8.96	N	Pure SOA	
LEV2-4.2	2010	4.06	13.63	N	Pure SOA	
D4.1	2005	4.19	5.19	Y	2	
D4.2	2005	1.16	11.1	Y	2	
LEV2-2.1	2008	4.18	12.63	N	Pure SOA	
D5.1	2001	0.68	5.29	Y	2	
D5.2	2001	3.78	14.63	Y	2	
D5.3	2001	3.20	12.04	Y	2	
LEV2-3.1	2008	3.24	6.42	N	Pure SOA	
LEV2-3.2	2008	3.31	5.89	N	Pure SOA	

ACPD
13, 24263–24300, 2013

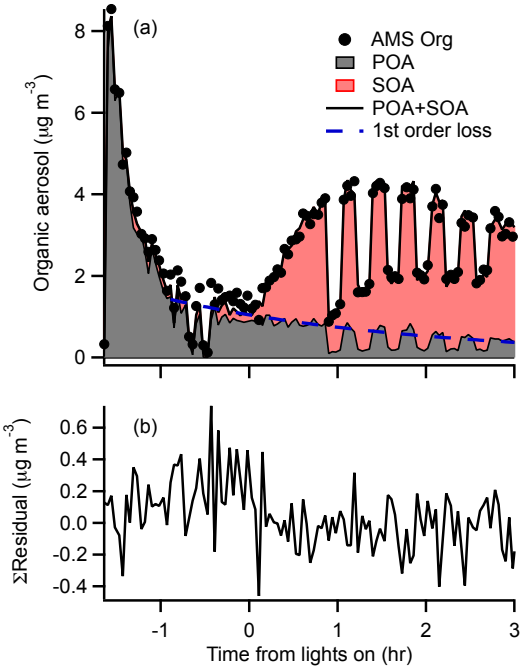

Fig. 1. Panel **(a)** shows a time series of a typical experiment (LEV1-5.2). Diluted exhaust was introduced to the chamber starting at $t = -1.4$ h (1.4 h before the start of photo-oxidation). Chamber filling ended at $t = -0.74$ h. The POA was characterized for approximately 45 min prior to the start of photo-oxidation at $t = 0$. The observed OA concentration increased after the start of oxidation, indicating production of SOA. The colors indicate the POA and SOA factors determined from PMF analysis. Modulations in the OA concentration indicate periods when the aerosol was sampled through a thermodenuder. The blue dashed line shows a predicted first-order wall loss rate for POA based on black carbon wall loss. Panel **(b)** shows the residual of the PMF solution.

ACPD
13, 24263–24300, 2013

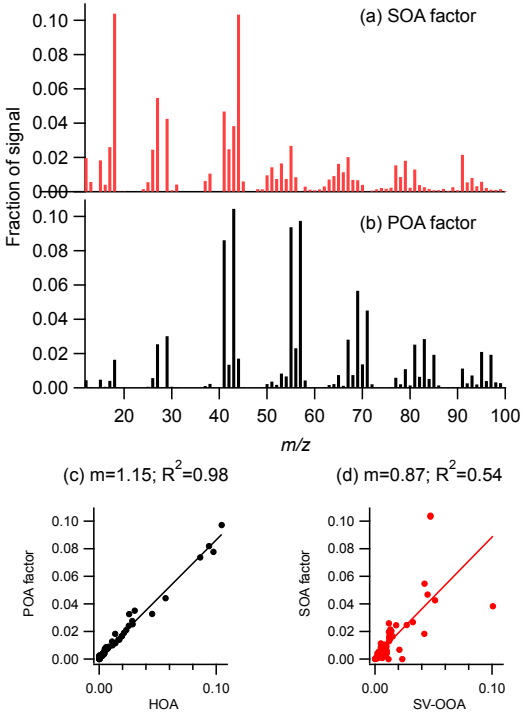

Fig. 2. Mass spectra of the PMF factors for **(a)** SOA and **(b)** POA for the experiment shown in Fig. 1. The POA factor is dominated by reduced ions C_xH_y. m/z 44 is the largest ion in the SOA mass spectrum. Panels **(c)** and **(d)** show comparisons of the POA mass spectrum to the ambient HOA factor and the SOA mass spectrum to the average ambient SV-OOA factor from Ng et al. (2011b).

ACPD
13, 24263–24300, 2013

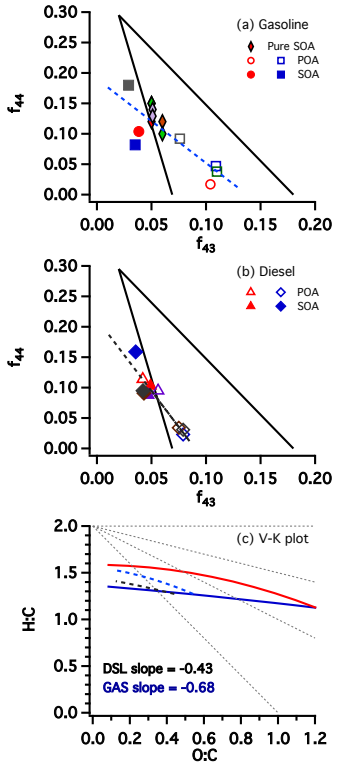

Fig. 3. Panels **(a)** and **(b)** show triangle plots for gasoline and diesel vehicle experiments. POA factors are shown as open symbols, and SOA factors as filled symbols. Filled symbols with a black border show "pure SOA" experiments for gasoline vehicles. The dashed lines are best fits through the data. Panel **(c)** shows a van Krevelen plot using the lines plotted in **(a)** and **(b)**. f_{44} and f_{43} are converted to O : C (Aiken et al., 2008) and H : C (Ng et al., 2011a) using published relationships.

ACPD
13, 24263–24300, 2013

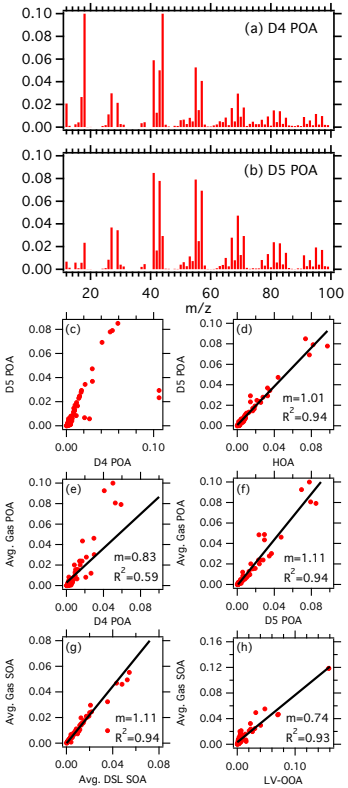

Fig. 4. Panels **(a)** and **(b)** show POA factors for vehicles D4 and D5. Panels **(c)** through **(h)** show scatter plots comparing the various gasoline and diesel POA and SOA factors to each other and to ambient HOA and LV-OOA factors. There is a high correlation between gasoline POA and POA from vehicle D5 **(f)**, as well as between gasoline and diesel SOA **(g)**, but poor agreement between the SOA factors and published mass spectra for ambient OOA **(h)**.

ACPD
13, 24263–24300, 2013

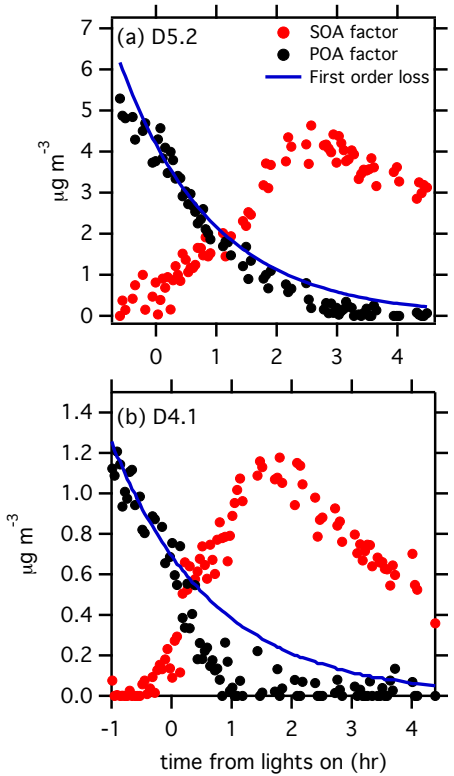

Fig. 5. Time series of the SOA (red) and POA (black) factors for experiments with vehicles **(a)** D5 and **(b)** D4. First-order wall loss based on black carbon decay is shown as a blue line. The POA in panel **(a)** decays according to a first-order wall loss rate for the entire experiment, whereas the POA in panel **(b)** evaporates for $t>0$.

ACPD
13, 24263–24300, 2013

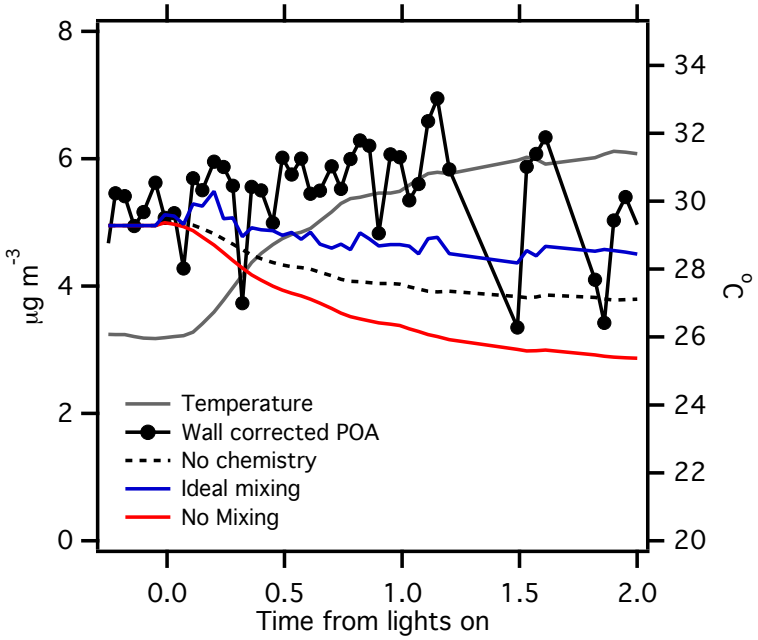

Fig. 6. Modeling results for the case shown in Fig. 5a. POA (black) data are based on AMS measurements and PMF analysis. Chamber temperature is shown as a grey line. Two modeling cases are shown. Case 1 (blue line) assumes ideal mixing between the POA and SOA. Case 2 (red line) assumes that the POA and SOA do not mix. The black dashed line is a version of Case 2 with no gas-phase chemistry ($k_{OH} = 0$) to show the effect of temperature on POA concentrations.

ACPD
13, 24263–24300, 2013